Neuron, Vol. 39, 353–359, July 17, 2003, Copyright ©2003 by Cell Press

Coupling of Total Hemoglobin Concentration, Oxygenation, and Neural Activity in Rat Somatosensory Cortex

Anna Devor,[1,*] Andrew K. Dunn,[1]
Mark L. Andermann,[1,2] Istvan Ulbert,[1,3]
David A. Boas,[1] and Anders M. Dale[1]
[1]Massachusetts General Hospital NMR Center
Harvard Medical School
Charlestown, Massachusetts 02129
[2]Program in Biophysics
Harvard Medical School
Boston, Massachusetts 02115
[3]Institute for Psychology of the Hungarian Academy of Sciences
Budapest 1068
Hungary

Summary

Recent advances in brain imaging techniques, including functional magnetic resonance imaging (fMRI), offer great promise for noninvasive mapping of brain function. However, the indirect nature of the imaging signals to the underlying neural activity limits the interpretation of the resulting maps. The present report represents the first systematic study with sufficient statistical power to quantitatively characterize the relationship between changes in blood oxygen content and the neural spiking and synaptic activity.

Using two-dimensional optical measurements of hemodynamic signals, simultaneous recordings of neural activity, and an event-related stimulus paradigm, we demonstrate that (1) there is a strongly nonlinear relationship between electrophysiological measures of neuronal activity and the hemodynamic response, (2) the hemodynamic response continues to grow beyond the saturation of electrical activity, and (3) the initial increase in deoxyhemoglobin that precedes an increase in blood volume is counterbalanced by an equal initial decrease in oxyhemoglobin.

Introduction

Neural activity changes in brain tissue are coupled to changes in blood flow, blood volume, and blood oxygenation, collectively referred to as the hemodynamic response. A number of brain imaging techniques, among them functional magnetic resonance imaging (fMRI), infer neural activity from hemodynamic changes (Kwong et al., 1992; Ogawa et al., 1992). However, the nature of the coupling between the fMRI signal and brain electrical activity is still under debate (Arthurs and Boniface, 2002; Heeger and Ress, 2002; Kim and Ogawa, 2002; Lauritzen, 2001). Many fMRI studies have relied on a linear coupling model, where the hemodynamic signal is assumed to be proportional to a measure of neural activity. If a linear relationship were a satisfactory approximation, this would greatly simplify the analysis and interpretation of fMRI data (Heeger and Ress, 2002). Indeed, a number of recent studies have provided evidence in support of a linear coupling model, showing that hemodynamic signals correlate linearly with synchronized synaptic activity (Arthurs et al., 2000; Brinker et al., 1999; Ngai et al., 1999) as well as with neural firing rates (Smith et al., 2002). Across-species comparison of single-cell activity in monkeys and human fMRI data also yielded a linear relationship (Heeger et al., 2000; Rees et al., 2000). However, these studies have generally had insufficient statistical power to detect subtle departures from linearity due to measurement noise, insufficient number of data points, or a narrow range of stimulus intensities. For instance, only two conditions were used in Smith et al. (2002). Ngai et al. (1999), on the other hand, used a much larger number of data points ($n = 34$). However, the measurement variance makes it difficult to distinguish between linear and nonlinear models. In the report by Logothetis et al. (2001), the dynamic range of the stimulus intensities may have been too narrow to reveal a nonlinear relationship. Furthermore, in order to reduce artifacts in the electrophysiological recordings introduced by simultaneous fMRI measurements, the analysis was limited to frequencies above 40 Hz.

Another potential problem is that the linear fits reported in several studies (Arthurs et al., 2000; Logothetis et al., 2001; Ngai et al., 1999) suggest a significant positive or negative change in the hemodynamic signal corresponding to the baseline level of electrophysiological activity. Since the hemodynamic response is measured as a change from baseline, the response to the absence of a stimulus (or zero stimulus amplitude) should be zero, and thus the curve would be expected to go through the origin.

The present report represents the first systematic study with sufficient statistical power to quantitatively characterize the nonlinear relationship between changes in blood oxygen content and the neural spiking and synaptic activity by employing high signal-to-noise ratio (SNR) hemodynamic measurements with rich data sampling over a wide range of neural response amplitudes.

Results

Spectroscopic optical measurements of total hemoglobin concentration and hemoglobin oxygenation (Dunn et al., 2003) were performed simultaneously with electrophysiological recordings in rat somatosensory (barrel) cortex. The barrel cortex in the rat is a well-studied example of topographic mapping, where each one of the large facial vibrissae (whiskers) is mapped onto a specific cortical area, called a barrel (Woolsey and Van der Loos, 1970). Tactile whisker stimulation produces neural and hemodynamic responses that localize to corresponding barrels (Masino et al., 1993). This system is perfectly suited for studying small and spatially localized cortical activations.

Single deflections of a single whisker produced a reliable hemodynamic signal with a spatial extent comparable to that reported in previous studies (Peterson et

*Correspondence: adevor@nmr.mgh.harvard.edu

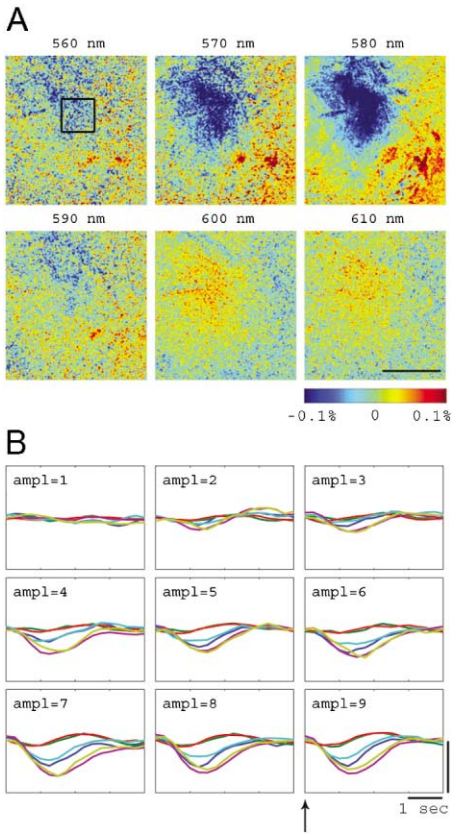

Figure 1. Multiwavelength Imaging of Intrinsic Signals

(A) Ratio images of activation for each of the 6 filters (wavelengths indicated above) were calculated by dividing the response (averaged 1.5–2.5 s following the stimulus) by the baseline image (averaged from 7 s preceding the stimulus). 990 trials were averaged for each stimulus amplitude. The signal is expressed in percent change from the baseline. Scale bar equals 500 μm.

(B) Signal time course for each of the 9 stimulus amplitudes, calculated by averaging the signal from the ROI (square in A, first panel). Responses for each of the 6 filters are superimposed. The stimulus onset is denoted by an arrow. Legend: 560 nm (dark blue), 570 nm (light green), 580 nm (purple), 590 nm (light blue), 600 nm (red), 610 nm (dark green). Vertical scale bar equals 0.2%.

al., 1998). Figure 1A shows ratio images obtained by dividing the maximal optical response image by the baseline image for the largest of the 9 stimulus amplitudes at each of the 6 wavelengths. The observed differences in signal sign and magnitude reflect absorption spectra of oxyhemoglobin (HbO) and deoxyhemoglobin (Hb). For example, imaging at 570 nm produces a map of total hemoglobin (HbT). It also reflects blood volume under the assumption of constant hematocrit. On the other hand, imaging at 610 nm creates a map highly biased toward Hb (Malonek and Grinvald, 1996). Figure 1B shows the averaged time course for each of the stimulus amplitudes measured from the region of interest (ROI) outlined by a square in Figure 1A. As expected, the amplitude of the response increased with stimulus intensity from stimulus amplitude 1 to 9.

Quantitative estimates of the concentrations of Hb, HbO, and HbT were obtained by fitting the observed signal changes at all wavelengths to a model, taking into account the respective absorption spectra (see Experimental Procedures). Figure 2 shows percent change maps for Hb, HbO, and HbT calculated from the spectral data in Figure 1. An initial increase in Hb (the "initial dip") was observed shortly following stimulus onset. The initial dip was originally reported by Grinvald and collaborators (Frostig et al., 1990) and since then has been observed by other groups (Thompson et al., 2003). In contrast to previous studies (Vanzetta and Grinvald, 2001), the initial increase in Hb was always balanced by an equal decrease in HbO, so that the blood volume (HbT) remained unchanged during the time of the initial dip. Blood volume started to increase about 600 ms following the stimulus, probably reflecting increased blood flow. As was first pointed out by Fox and Raichle (1986), an excessive delivery of fresh blood, measured in our study as an increase in blood volume, leads to an increase in HbO and decrease in Hb, HbO peaking before Hb (Figure 2).

Electrophysiological recordings of multiple unit activity (MUA) and local field potential (LFP) were performed simultaneously with optical measurements from the center of the barrel (Figure 3). LFP measures a weighted sum of transmembrane currents due to synaptic and dendritic activity (Eccles, 1951; Plonsey and Heppner, 1967), whereas MUA measures population spiking activity (Legatt et al., 1980; Mitzdorf, 1987). Both MUA and LFP showed a fast transient response followed by a delayed response with lower amplitude. This biphasic response has been observed in previous studies (Moore and Nelson, 1998) and has been attributed to the delayed activation of NMDA receptors (Armstrong-James et al., 1993).

MUA and LFP signals integrated over the time window of activation (ΣMUA and ΣLFP) increased as the stimulus intensity increased, and approached saturation at high stimulus amplitudes in each one of the animals (Figures 4A and 4B). The saturation was observed for the fast transient and the delayed responses components (Figures 4C and 4D).

In order to address the laminar patterns of electrophysiological activity, MUA and LFP were measured using a linear array multi-electrode (see Experimental Procedures). Current source density (CSD) analysis was performed on the LFP recodings, yielding laminar estimates of net transmembrane currents (Barth and Di, 1991; Mitzdorf and Singer, 1977; Nicholson and Freeman, 1975). Laminar distribution of MUA (Figure 4E) and CSD (Figure 4F) demonstrate that saturation was present in supragranular, granular, and infragranular layers.

To establish the relation between neural activity and hemodynamic signals, we compared ΣMUA and ΣLFP to peak responses of Hb, HbO, and HbT averaged from the ROI. In Figure 5, ΣMUA, ΣLFP, Hb, HbO, and HbT are averaged from 5 animals, and the error bars represent the intersubject standard error. ΣMUA (Figure 5A) and ΣLFP (Figure 5B) behaved in a similar way as a function of stimulus intensity. As a result, the relationship between ΣMUA and ΣLFP was close to linear (Figure 5C). The hemodynamic signals also increased with increasing stimulus intensity. However, in contrast to the electrophysiological parameters, there was no indication of saturation of the hemodynamic response at higher amplitudes (Figure 5D). As a result, the relation-

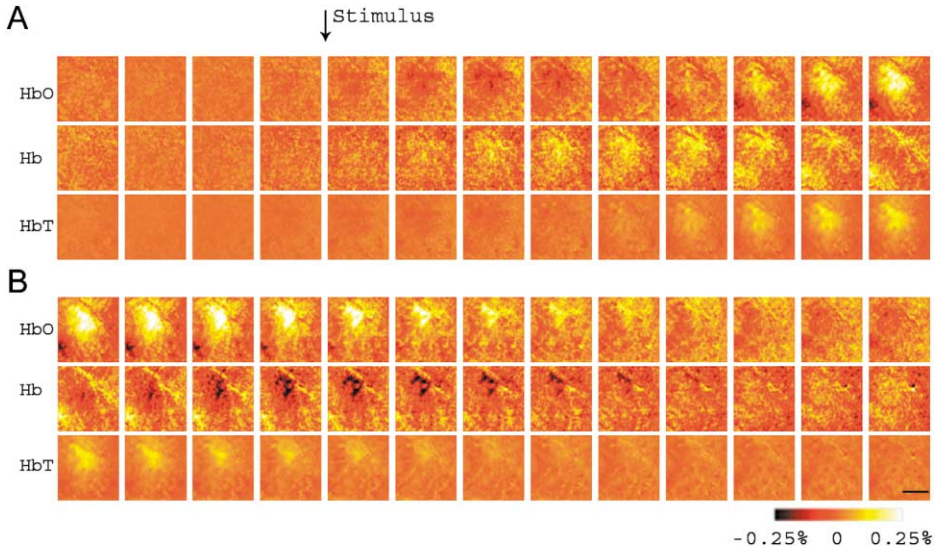

Figure 2. Spatial-Temporal Evolution of HbO, Hb, and HbT

Each image represents an individual frame (average of 990 trials). Time between consecutive images is 200 ms. (B) is a continuation of the time series shown in (A). The signal for Hb and HbO is expressed in percent change relative to its own baseline concentration (40 and 60 μM, respectively). HbT was calculated as a sum of Hb and HbO. Scale bar equals 500 μm.

ship between the observed electrophysiological measures and hemodynamic signals is nonlinear (Figure 5E).

The observed relationship between electrophysiological measures and the hemodynamic response amplitude can be well approximated by a power-law function

$$f = ax^b, \quad (1)$$

as shown in Figure 5E (solid lines). Note that a linear relation corresponds to $b = 1$. However, the value $b = 1$ falls far below the 95% confidence intervals for b shown above the plots, indicating a significant nonlinearity.

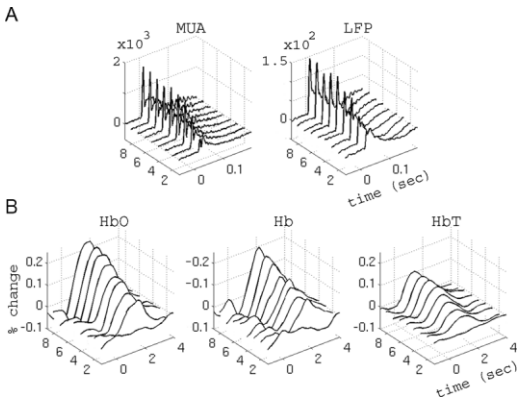

Figure 3. Simultaneous Recordings of Neural and Hemodynamic Signals

(A) MUA (expressed in spikes per second) and LFP (expressed in units of SD compared to the baseline) as a function of poststimulus time and amplitude (1–9).

(B) Signal time courses of Hb, HbO, and HbT calculated from the data in Figure 1B. Note that the Hb scale is inverted.

Discussion

Using simultaneous multiwavelength optical and electrophysiological recordings, we have demonstrated that (1) there is a strongly nonlinear relationship between electrophysiological measures of neuronal activity and the hemodynamic response, (2) the hemodynamic response continues to grow beyond the saturation of electrical activity, and (3) the initial increase in deoxyhemoglobin that precedes an increase in blood volume is counterbalanced by an equal initial decrease in oxyhemoglobin.

A number of improvements in experimental design can explain the disagreement between our results and previous studies that inferred a linear relationship. First, electrophysiological and hemodynamic signals were recorded simultaneously from the same cortical location (same barrel). Second, rapid and randomized event-related stimulus presentation methodology allowed a large number of stimulus trials (990 trials for each stimulus amplitude). This method is robust against slow drifts in baseline conditions. Data can therefore be acquired for long periods of time until the desired SNR level is reached. High reproducibility of the results allowed across-animal averaging. Likewise, high SNR and rich two-dimensional sampling of the hemodynamic data account for our ability to resolve the initial increase in Hb, which is accompanied by an initial decrease in HbO (Figure 2). This observation, which we interpret as reflecting a transition of HbO into Hb during the initial dip, is of particular importance for refining models of the coupling between blood flow and oxygen metabolism (Buxton, 2001).

Third, our use of a broad range of stimulus intensities allowed us to span the entire dynamic range of the electrophysiological response. The largest amplitude saturated the electrophysiological response but was still not

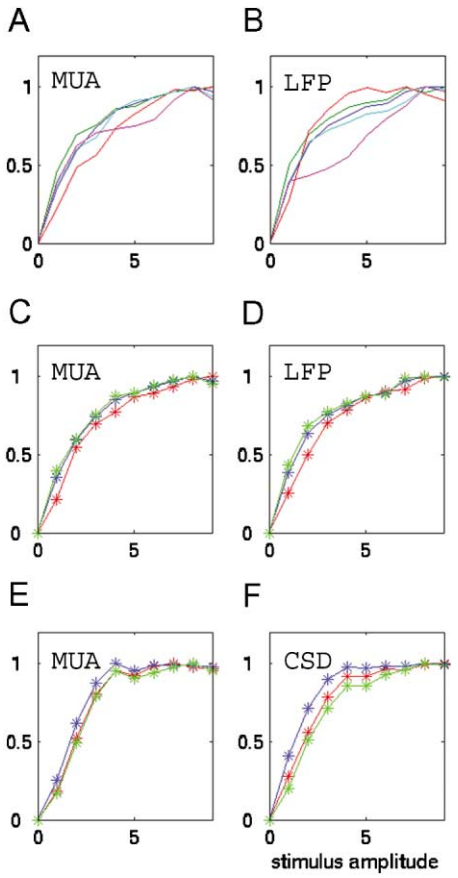

Figure 4. Saturation of Electrophysiological Measures

Each point is an average of 990 stimulus trials. Average responses were normalized to the maximal amplitude.

(A and B) MUA (A) and LFP (B) consistently saturate as a function of stimulus intensity. Responses for each of the 5 animals are superimposed.

(C and D) MUA and LFP saturate for both the transient and the delayed response components. The responses shown in Figure 3 were integrated 0–25 ms (red), 25–300 ms (green), and 0–300 ms (blue) following the stimulus.

(E and F) Averaged, rectifyed MUA (E) and CSD (F) recorded from supragranular layers (depth of 0–400 μm, red), granular layer (500–900 μm, blue), and infragranular layers (900–2000 μm, green).

large enough to reach a plateau of the hemodynamic response. In other sensory systems, such as the visual and auditory systems, stimulus intensities cover many orders of magnitude, and stimulus intensity is coded by the neural system logarithmically. In our system, mechanical constraints on whisker movement do not allow deflection amplitudes and velocities larger than those we used. It might be possible to reach hemodynamic plateau by adopting multiwhisker or electrical stimulation paradigms.

It has been proposed that neural metabolism is more closely linked to synaptic than spiking activity (Lauritzen, 2001; Logothetis, 2002). We are unable to address this question, since for the range of stimulus intensities used in the present study, LFP and MUA measures were highly correlated. However, our findings of continued hemodynamic increases beyond saturation of the electrophysiological measures are difficult to reconcile with hemodynamic activity driven by metabolic demands related to synaptic currents. In this context, it is important to note that LFP and MUA represent derived measures of neuronal activity and may in fact be nonlinearly related to other parameters such as ion pumping, neurotransmitter release, and vasoactive processes. Excess metabolic demand might also be attributed to nonneural cortical elements, for example astrocytes, which have high oxygen metabolism and release vasoactive compounds in response to neural neurotransmitter release (Zonta et al., 2003). Coupling between neural activity and hemodynamic signals confined to a well-defined dynamic range has been observed previously using laser Doppler flowmetry (Nielsen and Lauritzen, 2001) and in glucose consumption experiments (Ackermann et al., 1984). In the latter, within a certain domain, increased metabolism was accompanied not only by unchanged but decreasing neural activity. This result was interpreted as reflecting the metabolic demands of activating inhibitory circuits.

Our findings would be consistent with a saturating nonlinear relationship between neurotransmitter release and synaptic currents (e.g., due to the depolarization of postsynaptic membranes toward the reversal potential), and a roughly linear relationship between neurotransmitter release and the hemodynamic response. More formally, we would propose the following model:

$$y(t) = z(t) \otimes h(t),\ u(t) = S(z(t)), \tag{2}$$

where $y(t)$ and $u(t)$ are the measured hemodynamic and electrophysiological signals, respectively, as a function of time, t. $h(t)$ is a hemodynamic impulse response function, and $z(t)$ represents the neuronal process underlying the hemodynamic response and the measured neuronal signals (e.g., synaptic neurotransmitter release). The function S is a static saturating nonlinearity, as discussed above. By transforming the measured electrophysiological signals through the inverse of the static nonlinearity, we obtain the following expression

$$y(t) = S^{-1}(u(t)) \otimes h(t), \tag{3}$$

where S^{-1} is exactly the neurovascular coupling function given in Equation 1.

In order to relate this result to optical imaging or fMRI studies, consider an event-related experimental paradigm in which brief stimuli of various experimental conditions are presented in an arbitrary sequence. If the neuronal response to each stimulus of a given type or condition can be assumed to be time invariant (i.e., independent of stimulus history), Equation 3 can be closely approximated by the following linear expression

$$y(t) = \sum_{i}^{N} x_i(t) \otimes h_i(t), \quad h_i(t) = S^{-1}(u_i)h(t), \tag{4}$$

where $x_i(t)$ is the event sequence for condition i (a sum of delta functions, centered at the onset of each event; see Dale, 1999), u_i is the corresponding (time-integrated) electrophysiological response, and $h_i(t)$ is the event-related hemodynamic response function. Estimation of the $h_i(t)$ can be performed using standard linear estimation or deconvolution methods (Burock and Dale, 2000; Friston et al., 1998).

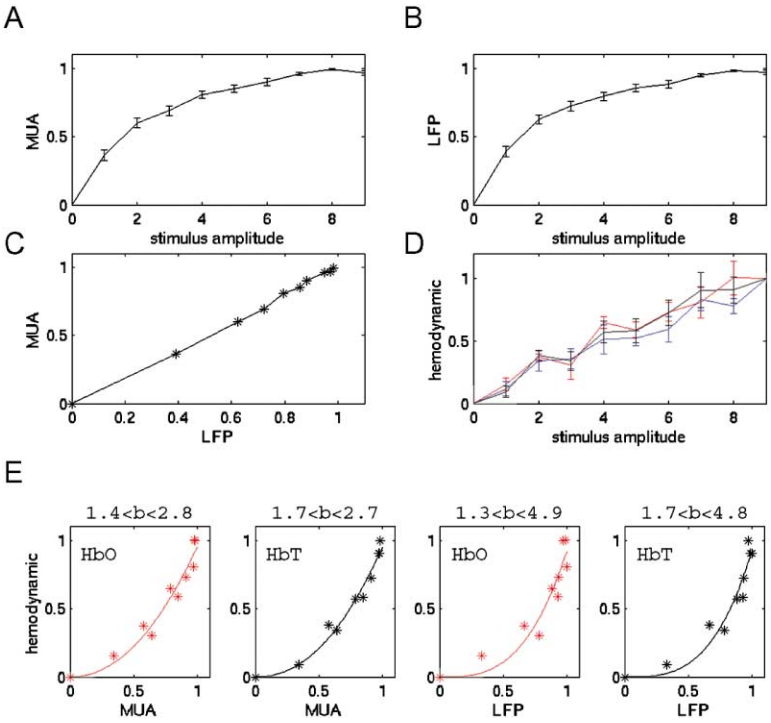

Figure 5. Nonlinearity of Neurovascular Coupling

Each point is an average of 4950 stimulus trials from 5 animals. Before averaging animals, ΣMUA, ΣLFP, Hb, HbO, and HbT responses to amplitude 9 was normalized to 1. The error bars represent intersubject standard error.

(A and B) ΣMUA (A) and ΣLFP (B) plotted as a function of stimulus intensity.

(C) ΣLFP as a function of ΣMUA.

(D) Hb (blue), HbO (red), and HbT (black) peak responses increase linearly with stimulus intensity.

(E) ΣLFP (right) and ΣMUA (left) as a function of the peak percent change in HbO (red) and HbT (black). A power-law function $f = ax^b$ was fit to the data (solid lines). Note that the hemodynamic response continues to grow beyond the plateau in ΣLFP and ΣMUA.

It has to be investigated whether our conclusions can generalize to other brain areas, other stimulus paradigms, and the awake versus anesthetized state. Lauritzen's group, using cerebellum as a model, has demonstrated an increase in the blood flow despite inhibition of Purkinje cells (Caesar et al., 2003). However, the large majority of the cells in the cerebellar cortex are granule cells, and the increase in blood flow might correspond to the increased activity in granule cell layer. Moreover, blood supply in the cerebellum is much richer in the granule cell layer than in the molecular layer (Scremin, 1995), probably corresponding to great density of granule cells.

Using our stimulus paradigm, recordings of neural responses from different layers produce similar stimulus-response functions. The similarity of responses in different layers may not necessarily hold for more complex, long-lasting, or multiwhisker, stimuli. Likewise, response properties of neurons are known to change as a function of type and depth of anesthesia (Friedberg et al., 1999; Martin et al., 2002). Further experiments in awake behaving animals will address these questions.

The integration of modern imaging techniques, such as fMRI, positron emission tomography, near-infrared spectroscopy, and electro/magnetoencephalography, offer great promise for noninvasive measurement of brain function in space and time (Dale and Halgren, 2001). The findings presented in this paper provide a principled basis for combining electrophysiological and hemodynamic measures through explicit mathematical modeling of the neurovascular coupling. Using brief and spatially localized stimuli and rich data sampling, we have demonstrated a strong nonlinear relationship between electrophysiological activity and the hemodynamic response. Further elucidation of the neurovascular relationship, including extension of our measurements to higher primates, can be expected to improve the accuracy and reliability of conclusions based on fMRI and may greatly facilitate the integration of multiple imaging modalities.

Experimental Procedures

Animal Preparation

All experimental procedures were conducted according to protocols approved by the Animal Care Committee. Five rats were used for simultaneous recordings of intrinsic optical signals and electrophysiological responses. Rats were anesthetized with urethane (1.2 g/kg, i.p.), and an area of skull overlying the primary somatosensory cortex was thinned with a dental burr until transparent (~100 μm). A barrier of petroleum jelly was built around the border of the thinned skull and filled with mineral oil. A small hole was made in the thinned skull over the center of a barrel, as determined by optical imaging, for insertion of the recording electrode. In addition, two rats were used for laminar electrophysiological recordings only. These animals were initially anesthetized with ketamine hydrochloride (50 mg/kg) supplemented with a single dose of sodium pentobarbital (12 mg/kg) during the surgery. During the rest of the experiment, the animal was supplemented by constant i.p. infusion of 50 mg/kg/hr of ketamine hydrochloride. The area of skull overlying the primary somatosensory cortex and the dura matter were removed, and the electrode array was slowly inserted into the cortex until the upper contacts showed stable recordings.

Spectroscopic Optical Imaging

To illuminate the cortex, light from a mercury xenon arc lamp was directed through a 6-position rotating filter wheel coupled to a 12 mm fiber bundle. We used 10 nm bandpass filters centered at wavelengths of 560, 570, 580, 590, 600, and 610 nm. The filterwheel rotated at ~3 Hz, thus producing ~18 independent illumination colors per second. Images were acquired by a cooled 12-bit CCD camera.

Reduction of spatially coherent noise in spectroscopic images was achieved by removing the first three temporal principal components, estimated from pixels well outside the ROI. These temporal components were projected out of the time course at every pixel prior to averaging. Trials corresponding to each stimulus type were

selectively averaged and blank (no stimulus) trial average was subtracted. This is formally equivalent to temporal deconvolution, given randomization of stimuli and sufficient number of trials (Dale, 1999; Dale and Buckner, 1997). Ratio images were calculated by dividing the response (averaged 1.5–2.5 s following the stimulus) by the baseline image (averaged from 7 s preceding the stimulus).

The spectral data were converted to percent change maps for Hb, HbO, and HbT using the modified Beer-Lambert law. Differential path length correction was applied to adjust for the differential optical path length through the tissue at different wavelengths (Kohl et al., 2000).

Electrophysiological Recordings

Electrophysiological recordings were performed using single metal microelectrodes (2–4 MΩ) placed in cortical layer IV or lower layer II/III in the center of a barrel. The position was identified by a selective response to the one whisker stimulated and by the cortical depth (400–500 μm). The electrode was positioned only once for each animal in order to preserve as much as possible of the thinned scull necessary for good quality optical measurements. The signals were amplified and filtered between 150 and 5000 Hz to record MUA, and between 0.1 and 500 Hz to record LFP. The MUA signal was subsequently high-pass filtered and thresholded for spike counting at 3 standard deviations (SD) above the baseline activity level, and therefore did not require rectification. ΣMUA and ΣLFP were calculated as an integral of the area under the response curve 0–0.3 s after the stimulus onset. Averaged LFP curves were rectified on the time axis before integration. Laminar recordings were performed using a linear array multielectrode with 24 contacts spaced at 100 μm (Ulbert et al., 2001a). Laminar signals were amplified and filtered between 500 and 5000 Hz to record MUA, and between 0.1 and 500 Hz to record LFP. CSD was full wave rectified and averaged across the traces falling in the corresponding laminae (supragranular, granular, and infragranular). Integration of CSD over time gives a simple measure of the total synaptic/transmembrane activity evoked by the stimulus (Givre et al., 1995). The same procedure was applied on the laminar MUA to obtain the total spiking activity (Ulbert et al., 2001b).

Since 1 s ISI (see below) is sufficient for relaxation of the electrophysiological activity using a single deflection stimulus (Petersen, 2002), there was virtually no temporal overlap in the neural response.

Stimulation Paradigm

A single whisker was deflected by a computer-controlled piezoelectric stimulator. The stimulator, positioned 3 mm from the base of a whisker, deflected a whisker upward and allowed a free return to the resting position. The stimulus consisted of a single deflection of varying amplitude (from 1 to 9). Brief whisker deflections of constant duration (20 ms) were used in order to minimize shape differences of electrophysiological responses to different stimulus amplitudes. The angular velocity increased from 203°/s (vertical displacement of 240 μm, amplitude 1) to 969°/s (vertical displacement of 1200 μm, amplitude 9). Intervening stimulus amplitudes were spaced with equal increments on a linear scale.

We employed a fast, randomized event-related stimulus presentation paradigm analogous to that used in event-related fMRI studies (Burock et al., 1998; Wagner et al., 1998). We used a constant interstimulus interval (ISI) of 1 s, including blank trials. The stimulus sequence was optimized for event-related response estimation efficiency using the approach described by Dale (1999). The inclusion of blank trials (or "null events") is equivalent to drawing the ISI between nonblank events from a discrete random distribution (Burock et al., 1998).

Acknowledgments

We thank Eric Halgren and Stephanie R. Jones for critical reading of the manuscript. This work was supported by NIH R01 EB00790-01A2, NIH R01 RR13609, NIH P41 RR14075, NIH R01 NS044623, and the Mental Illness and Neuroscience Discovery (MIND) Institute.

Received: March 18, 2003
Revised: May 16, 2003
Accepted: June 16, 2003
Published: July 16, 2003

References

Ackermann, R.F., Finch, D.M., Babb, T.L., and Engel, J., Jr. (1984). Increased glucose metabolism during long-duration recurrent inhibition of hippocampal pyramidal cells. J. Neurosci. *4*, 251–264.

Armstrong-James, M., Welker, E., and Callahan, C.A. (1993). The contribution of NMDA and non-NMDA receptors to fast and slow transmission of sensory information in the rat SI barrel cortex. J. Neurosci. *13*, 2149–2160.

Arthurs, O.J., and Boniface, S. (2002). How well do we understand the neural origins of the fMRI BOLD signal? Trends Neurosci. *25*, 27–31.

Arthurs, O.J., Williams, E.J., Carpenter, T.A., Pickard, J.D., and Boniface, S.J. (2000). Linear coupling between functional magnetic resonance imaging and evoked potential amplitude in human somatosensory cortex. Neuroscience *101*, 803–806.

Barth, D.S., and Di, S. (1991). Laminar excitability cycles in neocortex. J. Neurophysiol. *65*, 891–898.

Brinker, G., Bock, C., Busch, E., Krep, H., Hossmann, K.A., and Hoehn-Berlage, M. (1999). Simultaneous recording of evoked potentials and T2*-weighted MR images during somatosensory stimulation of rat. Magn. Reson. Med. *41*, 469–473.

Burock, M.A., and Dale, A.M. (2000). Estimation and detection of event-related fMRI signals with temporally correlated noise: a statistically efficient and unbiased approach. Hum. Brain Mapp *11*, 249–260.

Burock, M.A., Buckner, R.L., Woldorff, M.G., Rosen, B.R., and Dale, A.M. (1998). Randomized event-related experimental design allow for extremely rapid presentation rates using functional MRI. Neuroreport *9*, 3735–3739.

Buxton, R.B. (2001). The elusive initial dip. Neuroimage *13*, 953–958.

Caesar, K., Gold, L., and Lauritzen, M. (2003). Context sensitivity of activity-dependent increases in cerebral blood flow. Proc. Natl. Acad. Sci. USA *100*, 4239–4244.

Dale, A.M. (1999). Optimal experimental design for event-related fMRI. Hum. Brain Mapp. *8*, 109–114.

Dale, A.M., and Buckner, R.L. (1997). Selective averaging of rapidly presented individual trails using fMRI. Hum. Brain Mapp. *5*, 329–340.

Dale, A.M., and Halgren, E. (2001). Spatiotemporal mapping of brain activity nby integration of multiple imaging modalities. Curr. Opin. Neurobiol. *11*, 202–208.

Dunn, A.K., Devor, A., Bolay, H., Andermann, M.L., Moskowitz, M.A., Dale, A.M., and Boas, D.A. (2003). Simultaneous imaging of total cerebral hemoglobin concentration, oxygenation, and blood flow during functional activation. Opt. Lett. *28*, 28–30.

Eccles, J.C. (1951). Interpretation of action potentials evoked in the cerebral cortex. Electroencephalogr. Clin. Neurophysiol. *3*, 449–464.

Heeger, D.J., and Ress, D. (2002). What does fMRI tell us about neuronal activity? Nat. Neurosci. Rev. *3*, 142–151.

Heeger, D.J., Huk, A.C., Geisler, W.S., and Albrecht, D.C. (2000). Spikes versus BOLD: what does neuroimaging tell us about neuronal activity? Nat. Neurosci. *3*, 631–633.

Fox, P.T., and Raichle, M.E. (1986). Focal physiological uncoupling of cerebral blood flow and oxidative metabolism during somatosensory stimulation in human subjects. Proc. Natl. Acad. Sci. USA *83*, 1140–1144.

Friedberg, M.H., Lee, S.M., and Ebner, F.F. (1999). Modulation of receptive field properties of thalamic somatosensory neurons by the depth of anesthesia. J. Neurophysiol. *81*, 2243–2252.

Friston, K.J., Flethcher, P., Josephs, O., Holmes, A., Rugg, M.D., and Turner, R. (1998). Event-related fMRI: characterizing differential responses. Neuroimage *7*, 30–40.

Frostig, R.D., Lieke, E.E., Ts'o, D.Y., and Grinvald, A. (1990). Cortical functional architecture and local coupling between neuronal activity and the microcirculation revealed by in vivo high-resolution imaging of intrinsic signals. Proc. Natl. Acad. Sci. USA *87*, 6082–6086.

Givre, S.J., Arezzo, J.C., and Schroeder, C.E. (1995). Effects of wavelength on the timing and laminar distribution of illuminance-evoked activity in macaque V1. Vis. Neurosci. *12*, 229–239.

Kim, S.G., and Ogawa, S. (2002). Insights into new techniques for high resolution functional MRI. Curr. Opin. Neurobiol. *12*, 607–615.

Kohl, M., Lindauer, U., Royl, G., Kuhl, M., Gold, L., Villringer, A., and Dirnagl, U. (2000). Physical model for the spectroscopic analysis of cortical intrinsic optical signals. Phys. Med. Biol. *45*, 3749–3764.

Kwong, K.K., Belliveau, J.W., Chesler, D.A., Goldberg, I.E., Weisskoff, R.M., Poncelet, B.P., Kennedy, D.N., Hoppel, B.E., Cohen, M.S., Turner, R., et al. (1992). Dynamic magnetic resonance imaging of human brain activity during primary sensory stimulation. Proc. Natl. Acad. Sci. USA *89*, 5675–5679.

Lauritzen, M. (2001). Relationship of spikes, synaptic activity, and local changes of cerebral blood flow. J. Cereb. Blood Flow Metab. *21*, 1367–1383.

Legatt, A.D., Arezzo, J., and Vaughan, H.G.J. (1980). Averaged multiple unit activity as an estimate of phasic changes in local neuronal activity: effects of volume-conducted potentials. J. Neurosci. Methods *2*, 203–217.

Logothetis, N.K. (2002). The neural basis of the blood-oxygen-level-dependent functional magnetic resonance imaging signal. Philos. Trans. R. Soc. Lond. B Biol. Sci. *357*, 1003–1037.

Logothetis, N.K., Pauls, J., Augath, M., Trinath, T., and Oeltermann, A. (2001). Neurophysiological investigation of the basis of the fMRI signal. Nature *412*, 150–157.

Malonek, D., and Grinvald, A. (1996). Interactions between electrical activity and cortical microcirculation revealed by imaging spectroscopy: implications for functional brain mapping. Science *272*, 551–554.

Martin, C., Berwick, J., Johnston, D., Zheng, Y., Martindale, J., Port, M., Redgrave, P., and Mayhew, J. (2002). Optical imaging spectroscopy in the unanaesthetised rat. J. Neurosci. Methods *120*, 25–34.

Masino, S.A., Kwon, M.C., Dory, Y., and Frostig, R.D. (1993). Characterization of functional organization within rat barrel cortex using intrinsic signal optical imaging through a thinned skull. Proc. Natl. Acad. Sci. USA *90*, 9998–10002.

Mitzdorf, U. (1987). Properties of the evoked potential generators: current source-density analysis of visually evoked potentials in the cat cortex. Int. J. Neurosci. *33*, 33–59.

Mitzdorf, U., and Singer, W. (1977). Laminar segregation of afferents to lateral geniculate nucleus of the cat: an analysis of current source density. J. Neurophysiol. *40*, 1227–1244.

Moore, C.I., and Nelson, S.B. (1998). Spatio-temporal subthreshold receptive fields in the vibrissa representation of rat primary somatosensory cortex. J. Neurophysiol. *8*, 2882–2892.

Ngai, A.C., Jolley, M.A., D'Ambrosio, R., Meno, J.R., and Winn, H.R. (1999). Frequency-dependent change in cerebral blood flow and evoked potentials during somatosensory stimulation in the rat. Brain Res. *837*, 221–228.

Nicholson, C., and Freeman, J.A. (1975). Theory of current source-density analysis and determination of conductivity tensor for anuran cerebellum. J. Neurophysiol. *38*, 356–368.

Nielsen, A.N., and Lauritzen, M. (2001). Coupling and uncoupling of activity-dependent increases of neuronal activity and blood flow in rat somatosensory cortex. J. Physiol. *533*, 773–785.

Ogawa, S., Tank, D.W., Menon, R., Ellermann, J.M., Kim, S.G., Merkle, H., and Ugurbil, K. (1992). Intrinsic signal changes accompanying sensory stimulation: functional brain mapping with magnetic resonance imaging. Proc. Natl. Acad. Sci. USA *89*, 5951–5955.

Petersen, C.C.H. (2002). Short-term dynamics of synaptic transmission within the excitatory neuronal network of rat layer 4 barrel cortex. J. Neurophysiol. *87*, 2904–2914.

Peterson, B.E., Goldreich, D., and Merzenich, M.M. (1998). Optical imaging and electrophysiology of rat barrel cortex. I. Responses to small single-vibrissa deflections. Cereb. Cortex *8*, 173–183.

Plonsey, R., and Heppner, D.B. (1967). Considerations of quasi-stationarity in electrophysiological systems. Bull. Math. Biophys. *29*, 657–664.

Rees, G., Friston, K., and Koch, C.A. (2000). Direct quantitative relationship between the functional properties of human and macaque V5. Nat. Neurosci. *3*, 716–723.

Scremin, O.U. (1995). Cerebral vascular system. In The Rat Nervous System, G. Paxinos, ed. (New York: Academic), pp. 3–35.

Smith, A.J., Blumenfeld, H., Behar, K.L., Rothman, D.L., Shulman, R.G., and Hyder, F. (2002). Cerebral energetics and spiking frequency: the neurophysiological basis of fMRI. Proc. Natl. Acad. Sci. USA *99*, 10765–10770.

Thompson, J.K., Peterson, M.R., and Freeman, R.D. (2003). Single-neuron activity and tissue oxygenation in the cerebral cortex. Science *299*, 1070–1072.

Ulbert, I., Halgren, E., Heit, G., and Karmos, G. (2001a). Multiple microelectrode-recording system for human intracortical applications. J. Neurosci. Methods *106*, 69–79.

Ulbert, I., Karmos, G., Heit, G., and Halgren, E. (2001b). Early discrimination of coherent versus incoherent motion by multiunit and synaptic activity in human putative MT+. Hum. Brain Mapp. *13*, 226–238.

Vanzetta, I., and Grinvald, A. (2001). Evidence and lack of evidence for the initial dip in the anesthetized rat: implications for human functional brain imaging. Neuroimage *13*, 959–967.

Wagner, A.D., Schacter, D.L., Rotte, M., Koutstaal, W., Maril, A., Dale, A.M., Rosen, B.R., and Buckner, R.L. (1998). Building memories: remembering and forgetting of verbal experiences as predicted by brain activity. Science *281*, 1188–1191.

Woolsey, T.A., and Van der Loos, H. (1970). The structural organization of layer IV in the region (SI) of mouse cerebral cortex. The description of a cortical field opposed of discrete cytoarchitectonic units. Brain Res. *17*, 205–242.

Zonta, M., Angulo, M.C., Gobbo, S., Rosengarten, B., Hossmann, K.A., Pozzan, T., and Carmignoto, G. (2003). Neuron-to-astrocyte signaling is central to the dynamic control of brain microcirculation. Nat. Neurosci. *6*, 43–50.